Chapter-2

Challenges in the Design of Ultr-Wideband Absorber: Misinterpretation of Reflective Polarization Converter as Wideband Absorber

2.1. Introduction

The study of metamaterial or metasurface-based absorber has gained attention after Landy *et al.* made the first experimental demonstration of a perfect metamaterial absorber with narrow bandwidth [22]. By using a double split-serration-rings (DSSRs) structure, a three-layer perfect metamaterial-inspired absorber was recently presented by Si-Jia-Li *et al.* [33]. In [33], the reported absorber performs wideband and multiband absorption for two different combinations of serration rings, respectively. However, a careful analysis of both configurations of the metamaterial-inspired structure reveals that it is not an absorbing structure, but a reflective polarization converter. The proposed structure exhibits an anisotropic geometry due to splits made in each serration ring in a particular manner. Therefore, it exhibits a high cross-polarized reflected component over the operating band that was neglected by authors in the calculation of absorptivity performance. As a result of this fact, the majority of such claimed absorbers are, in realty, reflective type cross-polarization converters [38], [39], [86]–[88]. Practically, it is very challenging to achieve wideband or ultra-wideband absorption with low loss metamaterials/metasurfaces or frequency selective surfaces.

2.2 Theory and Analysis

2.2.1 *Absorptivity and PCR estimation*

In this reported structure, from top to bottom, DSSR-I is placed between the first and second dielectric layers, and DSSR-II is placed between the second and third dielectric layers as shown in Fig. 2.1(a). The bottom of the reported absorber is a metallic layer. The perspective of absorber for two different configurations is illustrated in Fig. 2.1(b) and Fig. 2.1(c). The rotatory angle between splits center of DSSR-I and DSSR-II is represented by β. When $\beta = 90°$, split center of DSSR-I and DSSR-II is oriented

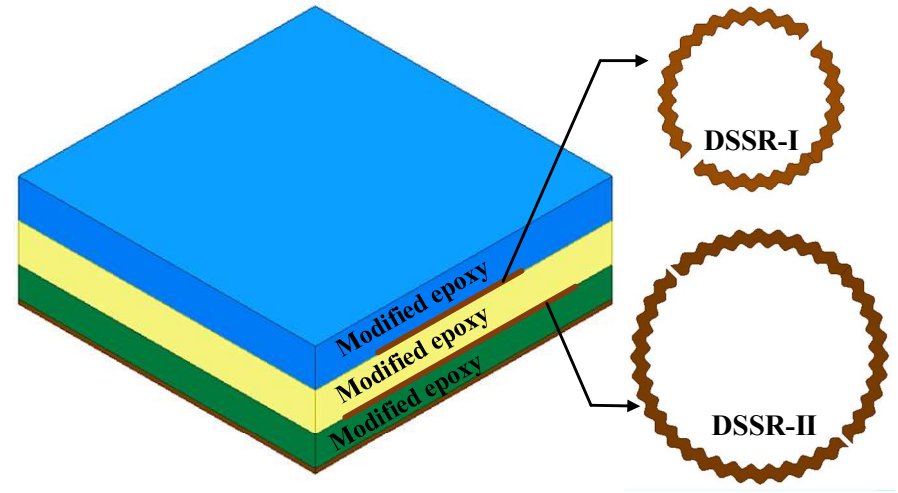

(a)

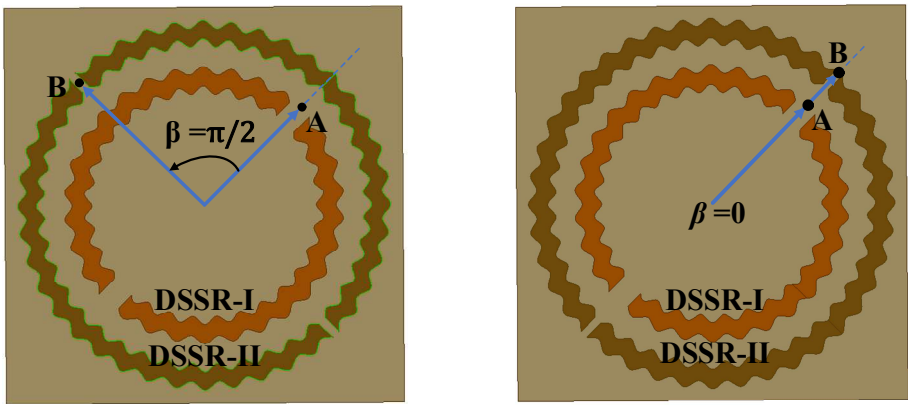

(b) (c)

Fig. 2.1: (a) Schematic of reported unit cell (b) Perspective of the absorber when split center of DSSR-I and DSSR-II is oriented perpendicular to each other (c) Perspective of the absorber when split center of DSSR-I and DSSR-II is oriented parallel to each other.

perpendicular to each other as depicted in Fig. 2.1(b). Similarly, in Fig. 2.1(c), when $\beta = 0°$, split center of DSSR-I and DSSR-II is oriented parallel to each other.

We have simulated once again the reported unit cell using high-performance computing (HPC) solutions ANSYS HFSS v. 2022 R2 software. The Floquet port excitation and periodic boundary condition are used in the simulation. Fig. 2.2 represents the magnitude of cross- and co- polarization reflection for both linearly *y*- (or TE) and *x*- (or TM) polarized incident wave. From the Fig. 2.2(a), for the $\beta = 90°$ case, the data shows that the

magnitude of co-polarized reflection is below -10 dB from 6.16 GHz–6.68 GHz and 9.84 GHz–15.14 GHz, which is in contrast to the claimed operating band of 5.34 GHz to 14.72 GHz. However, due to the anisotropic characteristic [89] of the proposed structure, it also exhibits high cross-polarized reflection higher than -1 dB from 6.16 GHz–6.68 GHz and 9.84 GHz–15.14 GHz. Similarly, from Fig. 2.2(b), for the β = 0° case, co-polarized reflection is lower than -10 dB and high cross-polarized reflection is higher than -1 dB over multiband.

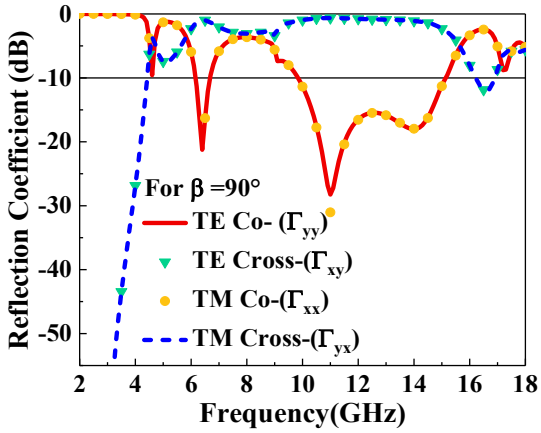

(a)

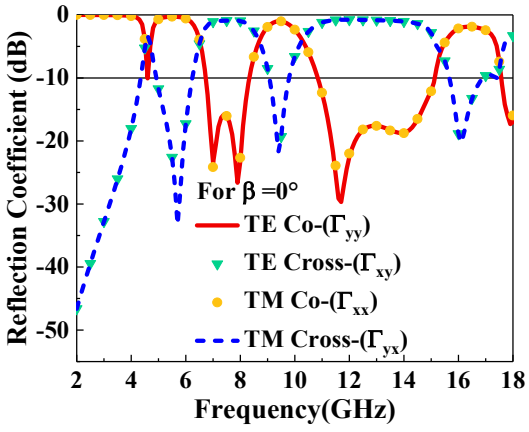

(b)

Fig. 2.2 Response of co- and cross- polarized reflection for both TE and TM polarized incident waves on the reported structure. (a) For β = 90° (b) β = 0°

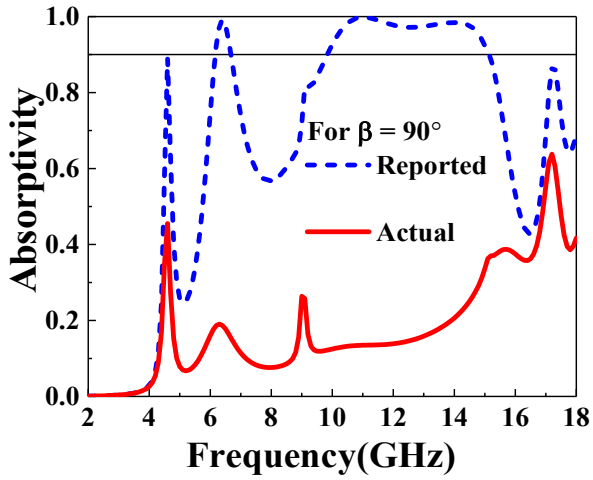

(a)

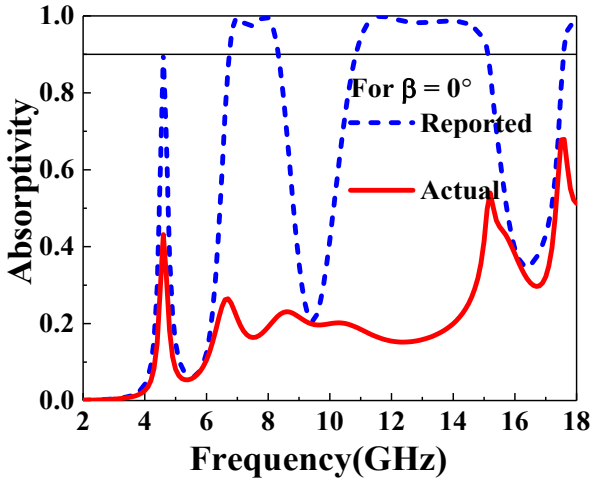

(b)

Fig. 2.3 Reported and actual absorptivity response of proposed absorber for y- (or TE) polarized incidence under normal incidence. (a) For $\beta = 90°$ (b) $\beta = 0°$

The absorptivity of the reported absorber over the operating band using the previously stated boundary condition is given by [38], [23]

$$A(\omega) = 1-|S^{11}(\omega)|^2-|S^{21}(\omega)|^2 \quad (2.1)$$

where, $|S^{11}(\omega)|^2=|\Gamma^{xy}(\omega)|^2+|\Gamma^{yy}(\omega)|^2$ represents the reflected and $|S^{21}(\omega)|^2=|\tau^{xy}(\omega)|^2+|\tau^{yy}(\omega)|^2$ transmitted power respectively. The cross- and co-polarized components of reflected and transmitted wave for linearly *y*- (or TE) polarized incident wave are represented with the subscript *xy* and *yy*. As the lower surface of the reported

absorber is made of metal, therefore $S^{21}(\omega)$ =0. Hence the absorbed power by the absorber is simplified by,

$$A(\omega) = 1 - |\Gamma^{xy}(\omega)|^2 - |\Gamma^{yy}(\omega)|^2 \quad (2.2)$$

The above expression indicates that to achieve maximum absorption from the absorber, it is essential to reduce both its cross-polarized and co-polarized reflected components.

By using expression (2.2), under the normal incidence, the actual absorptivity performance of the reported absorber for two different rotatory angles of β is presented in Fig. 2.3. For the $\beta = 90°$ case, it can be inferred that actual absorptivity is even less than 30 % over the claimed operating band, as shown in Fig. 2.3(a). In contrast, the absorptivity level greater than 90 % claimed by the authors is higher because they ignore the high cross-polarized reflected component in the absorptivity calculation. Moreover, as shown in Fig. 2.3(a), contrary to claimed wideband frequency response of 5.34–14.72 GHz, a noticeable dip in absorptivity level is also observed between 6.68 GHz–9.84 GHz when cross-polarized component is not included in the absorptivity estimation. The possible reason for this small variation in reported manuscript by Si-Jia-Li *et al.* may be due to minor differences in the simulation setup, such as geometric dimensions, material properties, or boundary conditions, as well as simulation accuracy, including meshing and convergence criteria. Similarly, for the $\beta = 0°$ case, actual absorptivity is below 30 % in most of multiband frequency regime as shown in Fig. 2.3(b).

To measure the efficiency of polarization conversion, the polarization conversion ratio (PCR) for *y*- polarized incident wave is given by

$$\mathrm{PCR} = \frac{|\Gamma^{xy}(\omega)|^2}{|\Gamma^{xy}(\omega)|^2 + |\Gamma^{yy}(\omega)|^2} \quad (2.3)$$

Using the above expression, PCR is plotted in Fig. 2.4. From Fig. 2.4(a), for the $\beta = 90°$ case, it can be observed that the PCR of the reported structure is greater than 0.9 and

hence more than 90 % between 6.17 GHz–6.68 GHz and 9.84 GHz–15.14 GHz. Similarly, for the $\beta = 0°$ case, the PCR of the reported structure is more than 90 % over multiband, as shown in Fig. 2.4(b). Therefore, the reported structure can be utilized as a highly efficient reflective-type polarization converter for both cases [86], [89], [90].

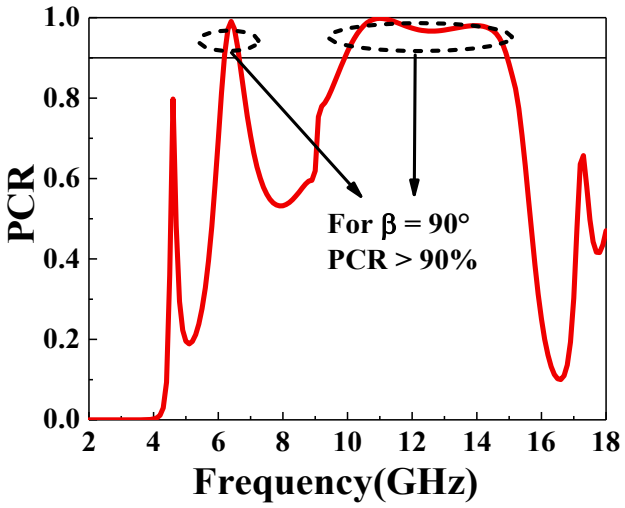

(a)

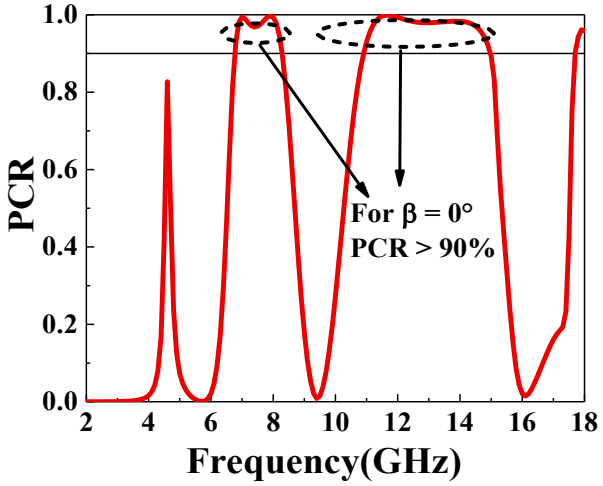

(b)

Fig. 2.4: PCR of reported structure for *y*-(or TE) polarized incidence wave under normal incidence (a) For $\beta = 90°$ (b) For $\beta = 0°$

2.2.2 *u-v analysis*

To acquire a better comprehension of the principle of polarization rotation, we have analyzed the reported anisotropic unit cell with mutually perpendicular symmetric *u*- and *v*- axes, marked along the ± 45° from the *y*- axis, as depicted in Fig. 2.5(a). Due to brevity, here we only analyzed the reported anisotropic unit cell geometry of $\beta = 90°$ case. Here *y*-axis is the direction of polarization for the incident wave. For polarization conversion analysis *y*-polarized incident field decomposed into *u*- and *v*- polarized fields [91]. Simulation is carried out for the reported structure for both *u*- and *v*-polarized fields. For the *u*-and *v*-polarized field, if r_{uu} and r_{vv} are reflected coefficient along *u*- and *v*- axes, then for polarization conversion there exists 180° phase difference ($\Delta\varphi = \pm 180°$) and unity amplitude ($r_{uu} = r_{vv} = 1$) among these coefficients [90], [91], [92]. Based on Fig. 2.5(b), it can be inferred that both r_{uu} and r_{vv} have nearly unity amplitude between two frequency ranges (6.17 GHz–6.68 GHz and 9.84 GHz–15.14 GHz), as shown in Fig. 2.5(b). However, the amplitude slightly reduced from unity due to some dielectric loss in the multilayer structure. The phase difference maintains roughly 180° between two frequency ranges (6.17 GHz–6.68 GHz and 9.84 GHz–15.14 GHz), as illustrated in Fig. 2.5(c). Therefore, the incident linearly *y*-polarized wave is converted into a reflected wave with orthogonal polarization over the above frequency range.

2.2.3 *Surface current distribution analysis*

To comprehend the physical mechanism [91] underlying polarization conversion, the simulated surface current distribution for $\beta = 90°$ case is plotted on the serration rings and metallic ground plane at the three resonance frequencies within the operating band, as depicted in Fig. 2.6. At each resonant frequency, the surface current

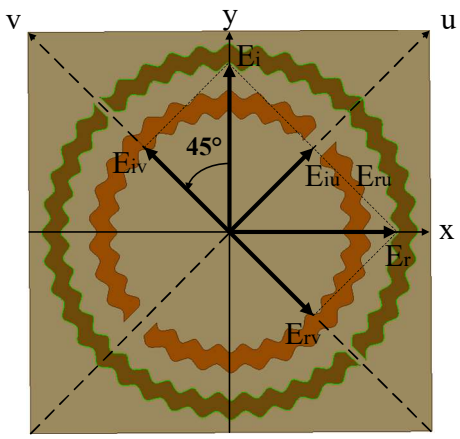

(a)

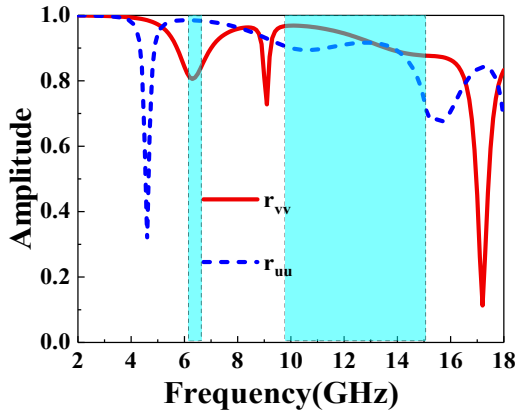

(b)

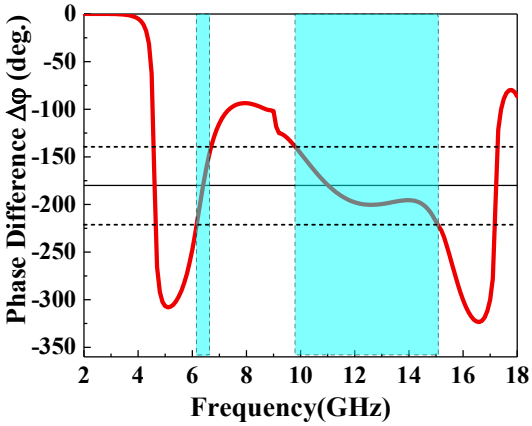

(c)

Fig. 2.5: Analysis of decompose *u*- and *v*-polarized field for *y*- (or TE) polarized incident wave for the case of DSSR-II is perpendicular to DSSR-I (a) *u*-*v* axis analysis (b) amplitude plot of r_{uu} and r_{vv} (c) phase difference response between r_{uu} and r_{vv}.

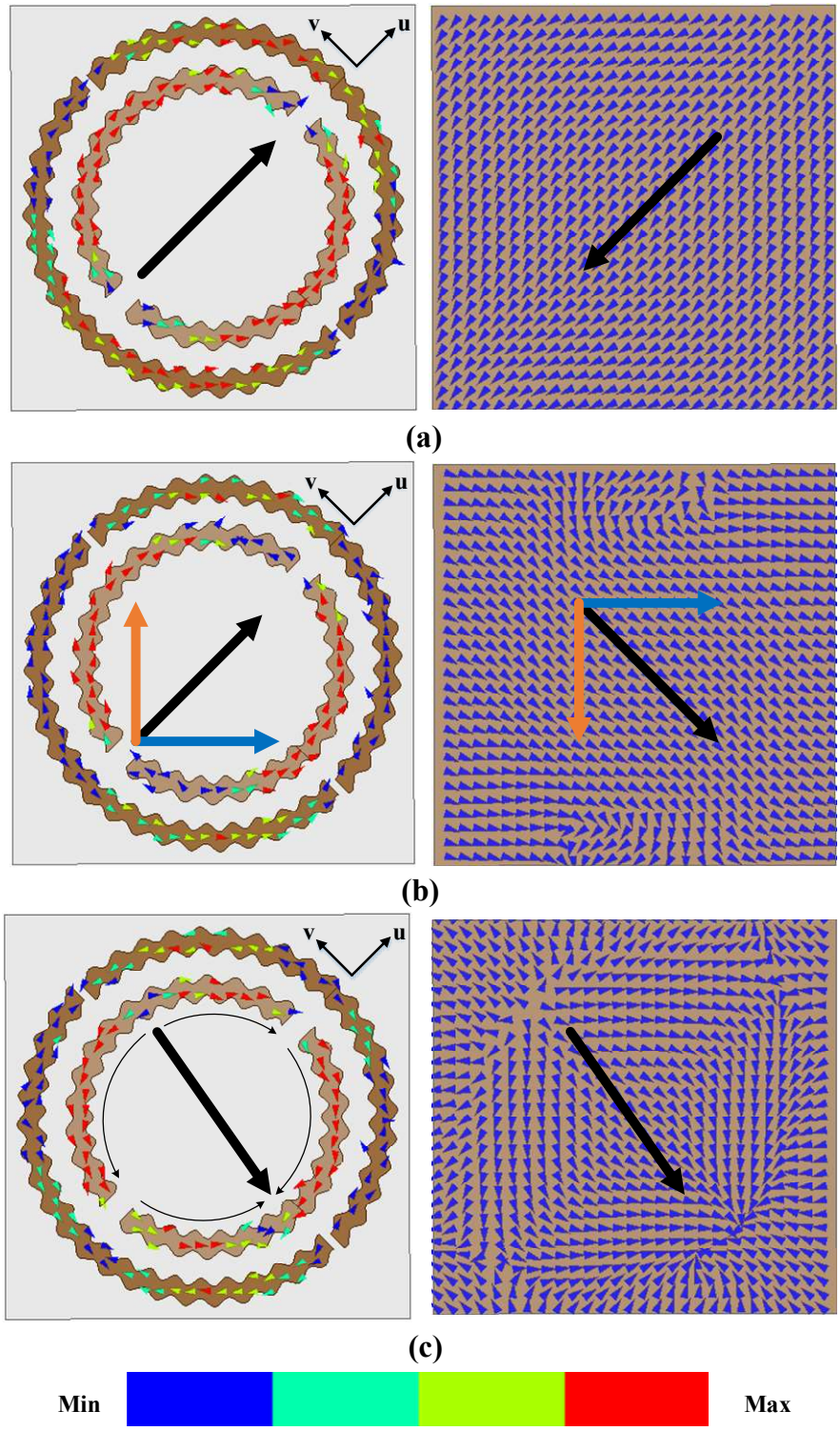

Fig. 2.6: For *y*- (or TE) polarized incident wave, the simulated surface current distribution on the serration rings (left) and metallic ground plane (right) at three resonant frequencies: (a) 6.3 GHz (b) 11 GHz (c) 14 GHz.

of the serration ring generates an induced current on the bottom metallic layer, which characterizes the resonant type. When *y*-polarized wave incident on the reported structure, strong current distribution is observed on DSSR-I at all three resonant frequencies, while weak current distribution is observed on DSSR-II. As depicted in Fig. 2.6(a), at 6.3 GHz, the resultant surface current on the top serration ring is opposite to the induced current at the metallic ground plane. It creates current loops in the substrate and thus excites the magnetic resonance. At 11 GHz, the induced currents on the ground plane are perpendicular to the resultant surface currents of the top serration ring, as shown in Fig. 2.6(b). Using vector decomposition, each of these resultant currents can be broken into two perpendicular components (shown by blue and orange arrows). The parallel vector component excites the electric resonance, while anti-parallel vector component excites the magnetic resonance. Hence, at 11 GHz, both magnetic and electric resonance are generated. Similarly, from Fig. 2.6(c), it can be observed that the resultant surface currents of the top serration ring are parallel to induced currents on the ground plane. As a result, at 14 GHz, there exists electric resonance. Furthermore, when the surface currents of DSSR-I and DSSR-II have the same direction, the coupling effect of the rings is reduced, and when they have opposite directions, the coupling effect is increased. Therefore, at 6.3 GHz, and 11 GHz, the unit cell is excited by the *u*- component, while at 14 GHz, it is excited by the *v*- component of the *y*- polarized incident field. Due to multi-resonant characteristic, the polarization converter operates over a wideband.

2.3 Conclusion

This work has shown that when estimating the absorptivity of structure, the cross-polarized reflected component of the incident wave cannot be neglected. Moreover, contrary to what the authors claimed, anisotropic structure is not a good option for an

efficient absorber. During the measurement, since the receiving and transmitting horn antenna are mounted in the same plane, cross-polarized reflection is not detected. One can measure cross-polarized reflection by rotating the receiving horn antenna 90° relative to the transmitting horn antenna [89]. The surface current distribution-based justification for significant absorption is no longer relevant, and reflective polarization conversion needs to be considered. The reported structure is not suitable for efficient absorption. However, it can indeed be utilized as a linear-type reflective polarization converter for both configurations of $\beta = 90°$ and $\beta = 0°$.